*Proceedings of the Thirty-second (2022) International Ocean and Polar Engineering Conference* **www.isope.org**
*Shanghai, China, June 5–10, 2022*

*ISBN 978-1-880653-81-4; ISSN 1098-6189*

# Numerical Study on Breaking Waves Interaction with Vertical Wall attached with Recurved Parapet

*Songtao Chen*[1], *Qingjie Meng*[2], *Decheng Wan*[1]*

[1] Computational Marine Hydrodynamics Lab (CMHL), School of Naval Architecture, Ocean and Civil Engineering, Shanghai Jiao Tong University, Shanghai, China
[2] Wuhan Second Ship Design and Research Institute, Wuhan, China
*Corresponding author

ABSTRACT

This paper numerically investigates breaking waves interaction with a vertical wall attached with a recurved parapet in 1:8 model scale. The in-house CFD solver naoe-FOAM-SJTU based on the open source platform OpenFOAM is used to perform the simulation. For wave generation, a novel generating-absorbing boundary condition (GABC) is adopted to replace the time-consuming moving boundary wavemaker. A geometric volume-of-fluid (VOF) method based on piecewise-linear interface calculation (PLIC) is incorporated in the present numerical model to capture the sharp interface and improve the accuracy of the predicted impact pressure. The time histories of the wave elevation and pressure at each probe are presented as well as the frequency analysis. In addition, the evolutions of free surface and pressure distribution are further provided to achieve a better understanding of this complex wave-structure interaction issue.

KEY WORDS: breaking waves; recurved parapet; naoe-FOAM-SJTU; generating-absorbing boundary condition (GABC); geometric VOF method

## INTRODUCTION

Vertical breakwaters are typical coastal structures intended to reduce the effects of incoming waves, especially in extreme sea conditions. In practical design, wave overtopping has been a significant issue of sustained concern for decades. Among the various solutions, a parapet fixed on the top of the vertical wall has been proven effective by deflecting back the up-rushing water seawards. However, according to the previous studies, the shape and parameters of the parapet will significantly influence the impact force and pressure compared with the original vertical wall. In order to provide guidelines to predict the wave impact and wave loading, it is necessary to systematically investigate the variations under different wave conditions, including non-breaking and broken waves.

As a representative shape, the recurved parapet has gradually attracted more attention recently. Kortenhaus et al. (2002, 2003) highlighted the effectiveness of the recurves and parapets in wave overtopping through abundant experimental data collected in the wave flume of the Leichtweiβ-Institute. Nevertheless, they pointed out that their existences may increase the wave loadings on the vertical wall. Ravindar et al. (2019) conducted large-scale (1:1) experiments to characterize the impact pressure under different wave breaking conditions at the Coastal Research Centre (FZK), Germany. According to their classification, it can be divided into three conditions: slightly breaking waves (SBW), breaking waves with small air trap (BWSAT), and breaking waves with large air trap (BWLAT). In addition, they reported the significant effect of the entrained air on the impact pressure. On this basis, Ravindar et al. (2021a, b) carried out small-scale (1:8) experiments in the Department of Ocean Engineering at the Indian Institute of Technology Madras, Chennai, Tamil Nadu, India. They analyzed the scale effects and proposed a combined Cuomo-Froude method for scaling up the impact pressure of small-scale results. Besides, they also discussed the impact pressure and forces of different types of parapets under the above-classified wave breaking conditions.

Considering the scale effect and the possible entrained air pocket, more and more scholars have adopted various numerical approaches to investigate the detailed behaviors of this problem. Castellino et al. (2018a, b) used the single-phase solver IH2VOF and the two-phase solver IHFOAM to conduct a series of two-dimensional simulations of a vertical breakwater with a recurved parapet under non-breaking waves. They identified an impulsive phenomenon referred to as “confined-crest impact” and further performed a sensitivity study on the parameters of the recurved parapet. Liu et al. (2019) used a two-phase compressible CFD solver with the Ghost Fluid Method (GFM) and a free surface turbulence model to explore the violent breaking wave impacts on a vertical wall. In their solver, the air compressibility was taken into account, thus being more physical under wave breaking conditions. Among four considered breaking conditions, they observed the maximum wave forces appear in the “flip-through” and “large air pocket” cases. Molines et al. (2020) numerically investigated the influence of parapets on crown walls of mound breakwaters with parapets based on OpenFOAM. Consistent with the previous studies, the dimensionless

horizontal forces and overturning moments increased with the presence of the parapet.

In the present study, the in-house CFD solver naoe-FOAM-SJTU is used to simulate the wave-structure interaction between breaking waves and a vertical wall attached with a recurved parapet in model scale, which is a part of the comparative study in the ISOPE-2022 conference. The primary objective is to validate the accuracy of naoe-FOAM-SJTU in simulating these violent free surface flows. The remainder of this paper is organized as follows. First, the numerical methods are introduced briefly, including the governing equations, interface capturing method, and wave generation approach. Then, the numerical setup is described in detail. In the following section, the results and discussion are presented in terms of the wave elevation, impact pressure, and flow field. Finally, the main conclusions are drawn.

## NUMERICAL METHODS

The in-house marine hydrodynamics CFD solver naoe-FOAM-SJTU based on the open source platform OpenFOAM is used to conduct the simulation. This solver consists of the self-developed six-degree-of-freedom (6DOF) rigid body motion module, Suggar-based dynamic overset grid module, and mooring line module. In addition, it also provides interfaces to a wide range of third-party libraries, including the wave2Foam, HOS-NWT, and HOS-ocean. Its accuracy and reliability have been validated in many complex practical problems, such as ship hull-rudder-propeller interaction, ship maneuverability, wave-structure interaction (WIC), vortex-induced motion (VIM), and so on (Wang et al., 2019; Shen et al., 2015; Wang and Wan, 2018; Cao and Wan, 2017; Zhao et al., 2018). Recently, the solver has been upgraded to the framework of OpenFOAM v8.

### Governing equations

In the present study, the flow is described by the two-phase incompressible Navier-Stokes equations as given below

$$\nabla \cdot \mathbf{U} = 0 , \tag{1}$$

$$\frac{\partial \rho \mathbf{U}}{\partial t} + \nabla \cdot \left( \rho \mathbf{U}\mathbf{U} \right) = -\nabla p_d - \mathbf{g} \cdot \mathbf{x} \nabla \rho + \nabla \cdot \left( \mu_{eff} \nabla \mathbf{U} \right) + f_\sigma , \tag{2}$$

where $\mathbf{U}$ is the velocity, $\rho$ is the weighted averaged density, $\mathbf{g}$ is the acceleration of gravity, and $\mathbf{x}$ is a coordinate vector, $p_d = p - \rho \mathbf{g} \cdot \mathbf{x}$ is the dynamic pressure, and $\mu_{eff}$ is the effective dynamic viscosity. $f_\sigma$ is the surface tension term defined as

$$f_\sigma = \sigma \kappa \nabla \alpha_v , \tag{3}$$

where the surface tension coefficient $\sigma$ is set to 0.07 N/m, $\kappa = -\nabla \left( \frac{\nabla \alpha_v}{|\nabla \alpha_v|} \right)$ is the interface curvature, and $\alpha_v$ is the phase fraction in the VOF method. Note that the laminar model is used throughout the simulation.

### Interface capturing method

To accurately capture the interface, the volume-of-fluid (VOF) method (Rusche, 2003) is adopted in the present study. The transport equation is given below

$$\frac{\partial \alpha_v}{\partial t} + \nabla \cdot \left( \alpha_v \mathbf{U} \right) = 0 , \tag{4}$$

where $\alpha_v$ is the phase fraction of the specified phase in each cell. Taking the air-water two-phase flow as an example, $\alpha_v$ = 1 and 0 represents the water and air, respectively. When $0 < \alpha_v < 1$, it represents the interface region between the water and air. In the following analysis, $\alpha_v = 0.5$ is regarded as the free surface to calculate the wave elevation at each probe.

In order to solve Eq. (4) without excessive numerical diffusion, a geometric VOF method based on piecewise-linear interface calculation (PLIC) is employed to obtain a sharp interface. It has already been available in OpenFOAM v8 as a series of new surface interpolation schemes for the phase fraction $\alpha_v$. Compared with other pure geometric methods, it can fall back to the interface-compression algebraic approach (Weller, 2008) when the interface cannot be fully resolved. This strategy can enhance robustness in dealing with practical engineering problems. For a detailed description, refer to the reference (Chen et al., 2022).

### Wave generation

In the present numerical model, a novel generating-absorbing boundary condition (GABC) is used for wave generation. This boundary condition has been implemented by Borsboom and Jacobsen (2021) in the third-party library wave2Foam (Jacobsen et al., 2012), based on the previous work by Wellens and Borsboom (2020). Compared with the original relaxation zone technique, it does not require the additional domain to dampen the waves at the outlet, thus saving computational cost. Moreover, this boundary condition is also capable of generating a variety of waves, including regular, irregular, and solitary waves.

The basic formulas are briefly introduced below. This boundary condition is based on the classical Sommerfeld radiation condition

$$\frac{\partial \phi}{\partial t} + c(z) \frac{\partial \phi}{\partial x} = 0 , \tag{5}$$

where $\phi$ is the velocity potential, and $c(z)$ is a depth-varying function instead of a constant, which is proposed for dispersive waves. When Eq. (5) is adapted into the Navier-Stokes framework, we can finally obtain a dynamic pressure condition

$$\begin{aligned} \left(1 + \frac{\rho c(z)}{\Delta} \left( \frac{1}{a_p} \right)_b \right) \left( p_d \right)_b = & \frac{\rho c(z)}{\Delta} \left( \frac{1}{a_p} \right)_b \left( p_d \right)_C \\ & + c(z) \rho \frac{\left( \mathbf{H}(\mathbf{u}_N) \right)_b}{\left( a_p \right)_b} - S_G \end{aligned} , \tag{6}$$

where $\rho$ is the weighted averaged density same as that in Eq. (2), $()_b$ denotes the variables on the boundary face, $()_C$ denotes the variables of the owner cell of the boundary face, $1/a_p$ is the diagonal coefficient of the semi-discretized form of Eq. (2), $\mathbf{H}(\mathbf{u}_N)$ consists of the source term and the contribution from all neighbor cells, and $S_G$ is the source term for wave generation. Although in the present working condition, wave absorption at the outlet is not required. Its low reflection coefficient achieved in different wave propagation cases has been validated in the references (Borsboom and Jacobsen, 2021).

## NUMERICAL SETUP

In the present study, the numerical setup is based on the wave flume

experiments that were performed in the Department of Ocean Engineering at the Indian Institute of Technology Madras, Chennai, Tamil Nadu, India.

**Computational domain and mesh**

Fig. 1 schematically shows the geometric model of the recurved parapet. Its arch is a quarter of a circle, so the horizontal length $H$ and vertical height $B$ are both 7.625 cm. In the experiments, this recurved parapet was fixed on the top of a vertical wall at the end of the wave flume, as shown in Fig. 2. In the present simulation, a two-dimensional computational domain with only one cell in the lateral direction ($y$-axis) is adopted to save computational cost. Other parameters are basically consistent with those of the wave flume. The origin of the coordinate system is at the intersection of the parapet and the free surface at still water. In Fig. 2(a), an overall view of the computational domain is presented. The distance between the inlet and the structure is 42.5 m, leaving a length of 2 m before the outlet. Fig. 2(b) further gives a magnified view near the parapet indicated by the red dashed box. The wave propagation region has a constant working depth of 0.5125 m, followed by a 1:10 slope in front of the parapet. The top of the computational domain is 0.4875 m above the still water, approximately with the working depth.

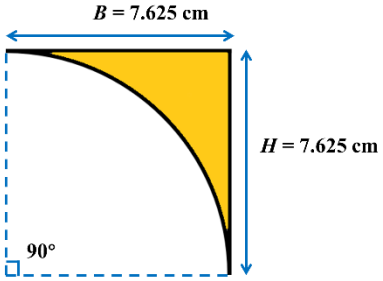


Fig. 1. Geometric model of recurved parapet.

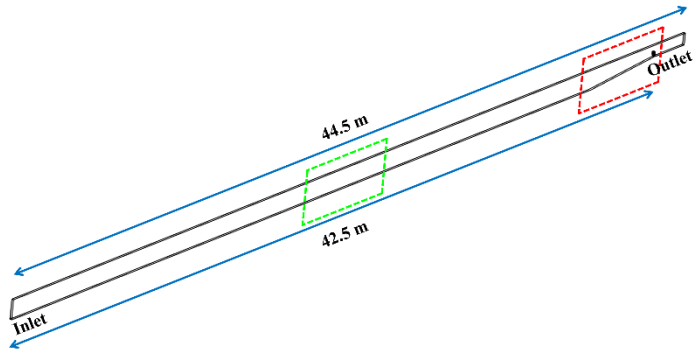


(a)

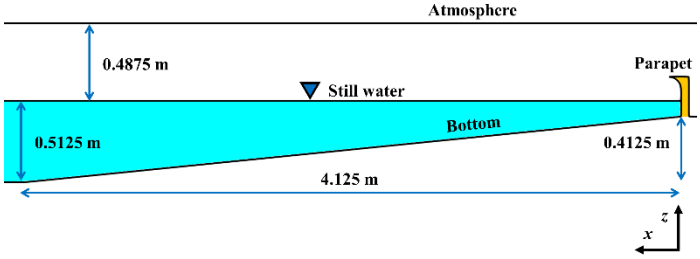


(b)

Fig. 2. Computational domain: (a) overview and (b) magnified view indicated by red dashed box.

In order to obtain a high-fidelity flow field, a two-dimensional block-structured mesh is adopted for simulation, as shown in Fig. 3. The bold black line represents the free surface at still water, and the red lines depict the topology of blocks. The present mesh consists of $4.6\times10^5$ cells, in which the configuration is mainly based on wave propagation in the far field and wave breaking in the near field.

Fig. 3(a) shows the magnified view of the wave propagation region indicated by the green dashed box in Fig. 2(a). The main purpose of the following mesh configuration is to minimize the numerical dissipation in wave propagation at a reasonable resolution, which is also well validated in Fig. 5. In the horizontal direction, the uniform length is approximately 1/115 $\lambda$, where $\lambda$ is the wavenumber. In the vicinity of the free surface, the uniform mesh height is approximately 1/30 $h$, where $h$ is the wave height. To save computational cost, the mesh gradually becomes coarse when approaching the atmosphere. However, given the present shallow water condition, the bottom effect cannot be ignored. Therefore, the height of the first near-wall layer on the bottom is set to $5\times10^{-4}$ m, and the corresponding expansion ratio is set to 1.3.

Fig. 3(b) further shows the magnified view near the recurved parapet, with the main focus on capturing such small-scale wave breaking phenomenon of interest. Three blocks are used to capture the feature edges of the vertical wall and parapet, which are blocks 1, 2, and 3, respectively. The height of the first near-wall layer is set to $4\times10^{-4}$ m, and the corresponding expansion ratio is set to 1.2. Moreover, to improve the aspect ratio, blocks 1 and 2 are of the higher mesh level in the vertical direction. This is mainly because of the wave breaking phenomenon that occurs in these regions. For the same reason, the cells in block 4 have a uniform size of $3\times10^{-3}$ m.

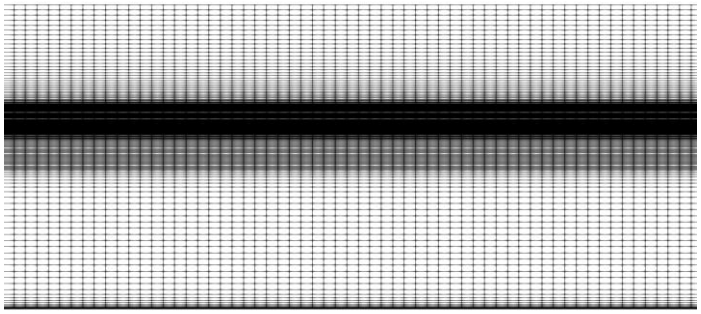

(a)

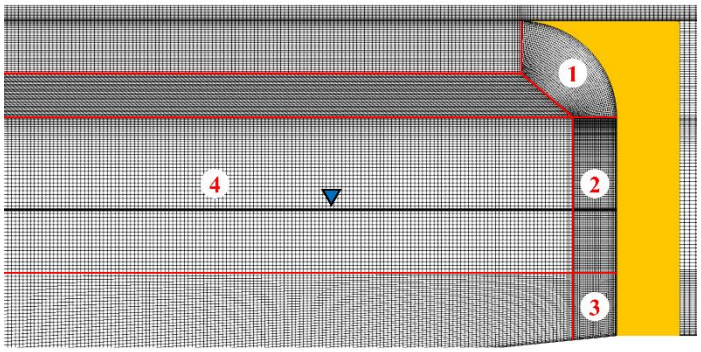


(b)

Fig. 3. Computational mesh: (a) magnified view of wave propagation region indicated by green dashed box and (b) magnified view near parapet indicated by red dashed box in Fig. 2(a).

**Working and Boundary conditions**

In the present study, the input wave is a monochromatic Stokes second-order regular wave with a wave height $h$ of 0.0875m and a wave period $T$ of 2.1 s. Moreover, according to the experimental setup, six wave probes are used to record the wave elevation $\eta$ at different positions, as listed in Table 1. Among them, the time history of wave elevation at WPB6 will be first compared with the theoretical solution to validate the GABC boundary condition. In addition, seven pressure probes, with four on the vertical wall ($x = 0$) and three on the recurved parapet ($x \neq 0$), are mounted on the structure to record the impact pressure. Table 2 lists their specific coordinates, and Fig. 4 further illustrates the relative positions on the structure.

Table 1. Location of wave probes

| Wave Probe | $x$ (m) |
|---|---|
| WPB1 | 0.83 |
| WPB2 | 4.62 |
| WPB3 | 5.08 |
| WPB4 | 5.66 |
| WPB5 | 11.5 |
| WPB6 | 24.5 |

Table 2. Location of pressure probes on structure

| Pressure Probe | $x$ (m) | $z$ (m) |
|---|---|---|
| PP1 | 0 | -0.075 |
| PP2 | 0 | -0.0325 |
| PP3 | 0 | 0.01 |
| PP4 | 0 | 0.0525 |
| PP5 | 0.005 | 0.1 |
| PP6 | 0.022 | 0.1262 |
| PP7 | 0.077 | 0.1475 |

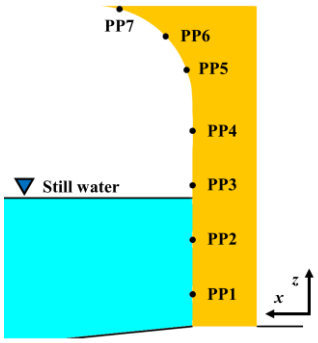


Fig. 4. Illustration of pressure probes on structure

For the boundary conditions, the GABC boundary condition is applied to the inlet for wave generation. The no-slip boundary condition is imposed on the structure and bottom, the Neumann boundary condition $\partial\varphi/\partial n = 0$ is used for the atmosphere and outlet, and the empty boundary condition is adopted for the lateral sides (not shown in Fig. 2).

For the temporal discretization, a blended scheme between the first-order Euler scheme and the second-order Crank-Nicolson scheme is adopted. The blending factor is set to 0.95 to avoid excessive numerical dissipation during wave propagation (Zhuang and Wan, 2021). For the spatial discretization, the second-order linear scheme is employed for the advection and diffusion terms in the momentum equation. Note that a PLIC corrected scheme is applied to the phase fraction transport equation. According to previous numerical studies under similar conditions (Castellino et al., 2018a; Liu et al., 2019), the maximum Courant–Friedrichs–Lewy number is usually in the range of 0.3 - 0.5. Therefore, an adjustable time step is used in this study to maintain a balance between accuracy and stability, which ensures the maximum Courant–Friedrichs–Lewy number is below 0.2 ($\Delta t \sim 10^{-5}$ s). The simulation time $t$ is 50 s, which gives sufficient periodic results for statistical analysis.

RESULTS AND DISCUSSION

**Wave elevation**

To validate the incident wave generation, Fig. 5 first shows the wave elevation at WPB6. In general, the result agrees well with the theoretical solution, demonstrating the good performance of the GABC boundary condition. The slight discrepancy in phase is possibly due to the cumulative numerical dissipation over a long distance and the reported spurious air velocities (Afshar, 2010).

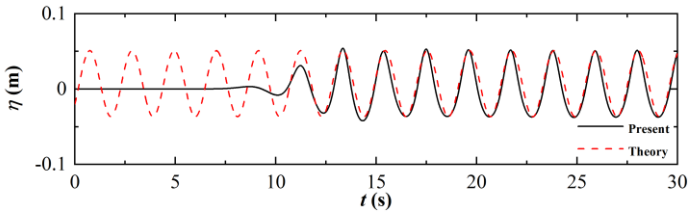


Fig. 5. Comparison of wave elevation at WPB6.

When the first wave front hits the structure, Fig. 6 shows the wave elevation at each probe to investigate the reflected wave characteristics between the next incident wave and the structure. The spectral analysis results are further given in Fig. 7 using the Fast Fourier Transform (FFT) method. When the locations are far from the structure, i.e., WPB5 and WPB6, Fig. 6(e) and (f) suggest the wave elevations are less affected by the reflected waves. Therefore, the dominant frequencies are still the significant first harmonic ($f_w$), as shown in Fig. 7(e) and (f). According to the increasing amplitudes in Fig. 6(c) and (d), the interaction between the incident and reflected waves becomes strong when approaching the structure. Moreover, it can be seen that small secondary peaks appear in the crests and troughs. This nonlinear phenomenon is manifested as growing high-order harmonics in Fig. 7(c) and (d). When closest to the structure, i.e., at WPB1, the oscillations appear in Fig. 6(a) because of the violent free surface deformation visualized later. In addition, periodic large-amplitude secondary peaks can be captured at WPB1. Consequently, the high-order harmonics increase rapidly, and higher components are newly identified in the spectrum (see Fig. 7(a)), including the $5^{th}$ and $6^{th}$ ones.

**Impact pressure**

In order to investigate the wave impact, the time-histories of pressure at each probe are given in Fig. 8. The left column is the overall views, and the right column is the magnified views during one impact. According to previous studies, a typical time history of pressure during one impact can be characterized as three parts in sequence: impact pressure, oscillatory pressure, and quasi-static pressure. Because PP1-3 are below or near the

free surface at still water, the water tongues of plunging breakers hit these positions directly. As a result, the impact peak pressure reaches very high within a short duration, as shown in Fig. 8(a)-(c).

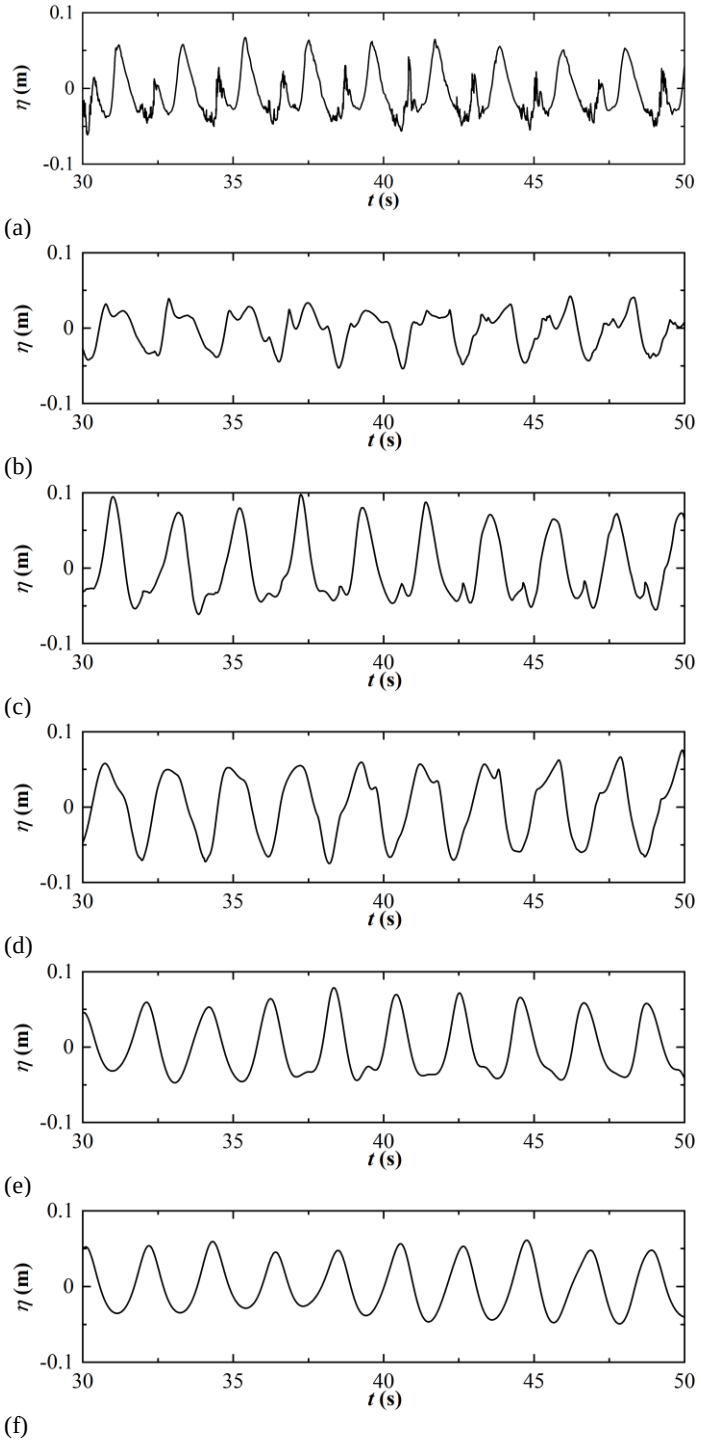


Fig. 6. Time histories of wave elevation at (a) WPB1, (b) WPB2, (c) WPB3, (d) WPB4, (e) WPB5, and (f) WPB6.

Then, the quasi-static stage is relatively long due to the sustained contact with the water. Moreover, in the present wave condition, the entrapped large air pocket (see Fig. 9) is responsible for the negative sub-atmospheric pressure, as indicated by the red arrow in Fig. 8(c). On the other hand, for the probes on the recurved parapet, i.e., PP5-7, the peak pressure is reduced, and the quasi-static stage becomes short due to the high-speed jet. However, the expected oscillatory pressure caused by the expansion and compression of the air pocket is not so obvious. To our knowledge, when air compressibility is further taken into account in the numerical model (Liu et al., 2019), this problem can be much improved. However, Liu et al. (2019) pointed out that even when considering air compressibility, the presence of air escape and dispersed air bubbles in the experiments would greatly affect the prediction of impact pressure. Therefore, it poses challenges to the interface capturing method, which should be improved in future high-fidelity numerical simulations. Furthermore, it is worth noting that the scale effect may also play an important role in air compressibility, which is also one of the main concerns in this ISOPE-2022 comparative test.

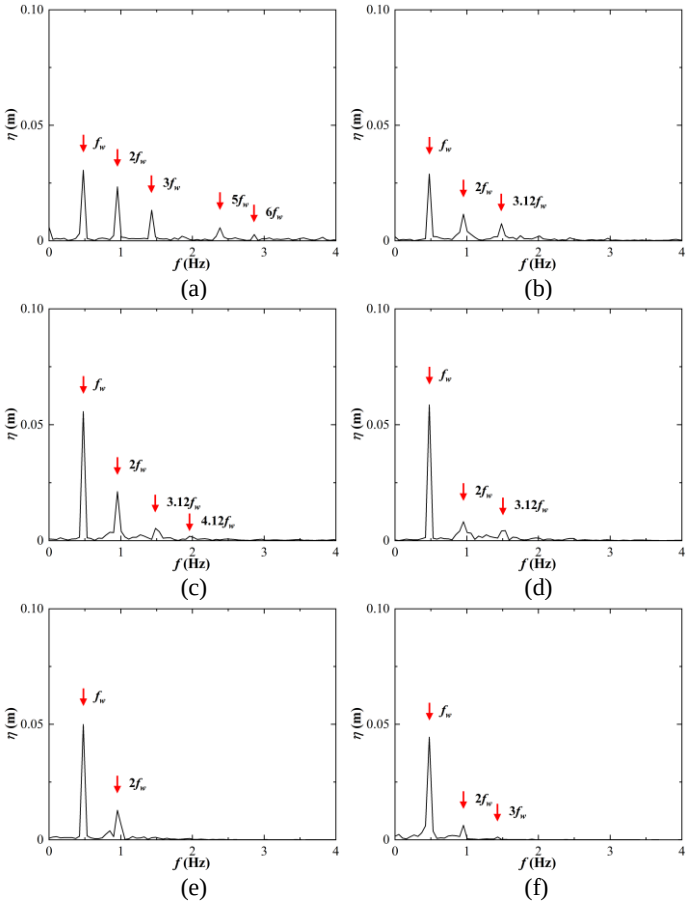


Fig. 7. Spectral analysis of wave elevation at (a) WPB1, (b) WPB2, (c) WPB3, (d) WPB4, (e) WPB5, and (f) WPB6.

**Flow field evolution**

To further explore the mechanism, the flow field evolution during one wave impact is visualized in this section. Fig. 9 shows the instantaneous free surface for a sequence of time instants, represented by the phase fraction $\alpha_v$. Correspondingly, Fig. 10 shows the contours of pressure. Here, the black points on the structure denote the above-listed pressure probes.

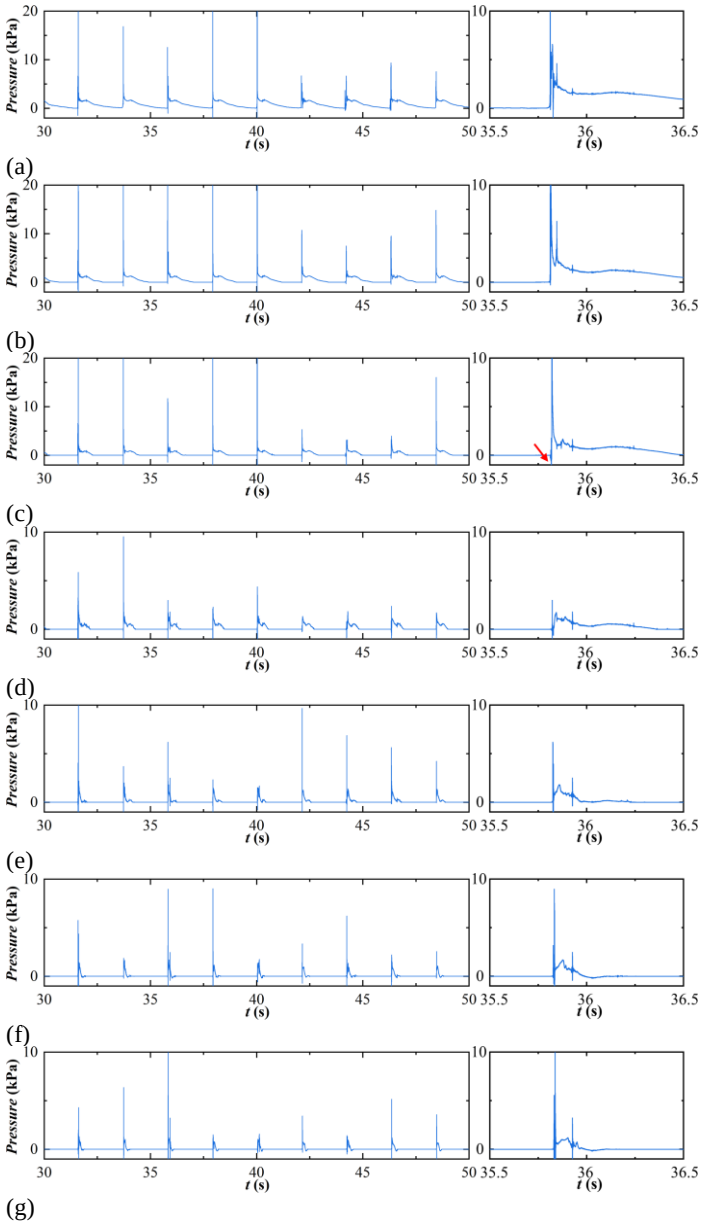


Fig. 8. Time histories of pressure at (a) PP1, (b) PP2, (c) PP3, (d) PP4, (e) PP5, (f) PP6, and (g) PP7.

Before reaching the structure, a plunging breaker has already been formed, as shown in Fig. 9(a). When the tongue of the plunging breaker subsequently hits the vertical wall, Fig. 9(b) shows that it entraps a lot of air and encloses up to form a large air pocket. With this feature, the present breaking condition belongs to a classified one proposed by Ravindar et al. (2019), i.e., breaking wave with a large air trap (BWLAT). Meanwhile, this impact by the wave tongues creates the high pressure regions colored dark pink, as shown in Fig. 10(b), which corresponds to the peak pressure in Fig. 8. After that, some water with high kinetic energy rises upwards rapidly along the vertical wall and hits the recurved parapet. Then, Fig. 9(d) shows that the up-rushing water is deflected back towards the incident direction by the parapet, resulting in a thin horizontal jet. At the same time, the entrapped large air pocket disperses into several small pockets and bubbles after expansion and compression. They are transported upwards with the water and collapse on the recurved parapet. These physical phenomena can well explain the negative sub-atmospheric pressure and the subsequent oscillation in Fig. 8. In Fig. 10, they appear as a chaotic distribution around the structure.

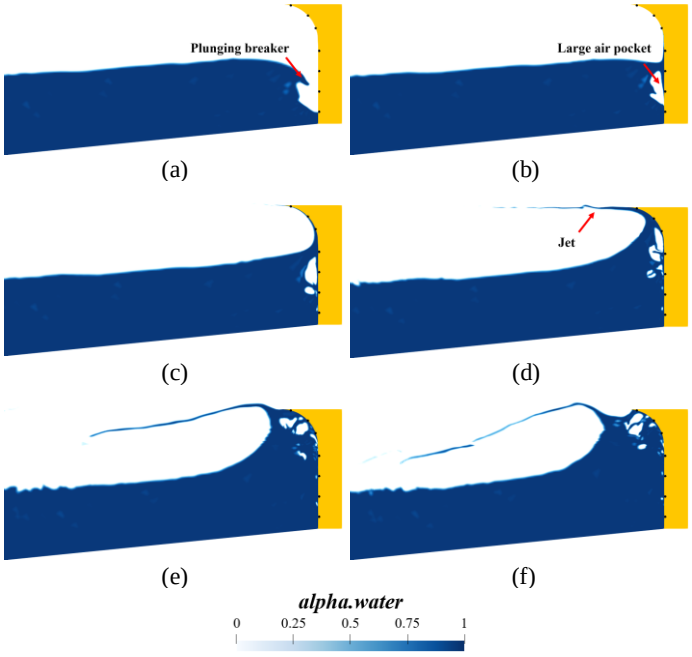


Fig. 9. Instantaneous free surface during one wave impact at (a) $t$ = 35.78 s, (b) $t$ = 35.8 s, (c) $t$ = 35.82 s, (d) $t$ = 35.86 s, (e) $t$ = 35.96 s, and (f) $t$ = 36.02 s.

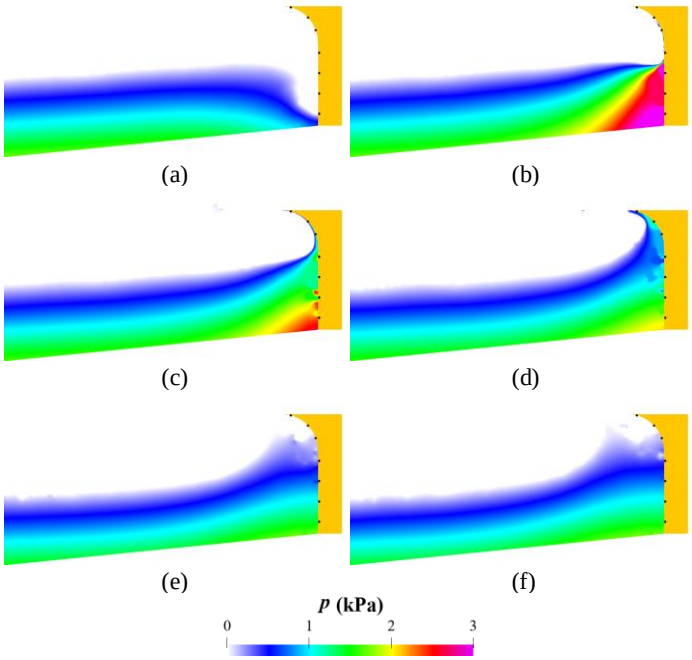


Fig. 10. Contours of pressure during one wave impact at (a) $t$ = 35.78 s, (b) $t$ = 35.8 s, (c) $t$ = 35.82 s, (d) $t$ = 35.86 s, (e) $t$ = 35.96 s, and (f) $t$ = 36.02 s.

## CONCLUSIONS

In this paper, the wave-structure interaction between breaking waves and a vertical wall attached with a recurved parapet is simulated by our in-house CFD solver naoe-FOAM-SJTU. For wave generation, a generating-absorbing boundary condition (GABC) is used to save computational cost. In order to capture a sharp interface, a PLIC-based geometric VOF method is adopted. At WPB6, the theoretical solution of the wave theory is first compared with the numerical results to validate the wave generation. Then, the time histories and contours of wave elevation and pressure are provided to analyze the reflection characteristics and wave impact. The main conclusions are as follows.

When the locations are far from the structure, the wave elevation is still dominated by the incident wave. However, when approaching the structure, the nonlinearity of wave elevation increases rapidly, which is manifested as significant high-order harmonics in the spectrum. This phenomenon is particularly evident at WPB1. For the impact pressure on the structure, a large-amplitude and short-duration peak can be observed below or near the free surface at still water. On the other hand, the wave impact on the recurved parapet can be characterized as reduced peak pressure and a short quasi-static stage. Visualization of the flow field further shows that after the tongue of the plunging breaker hits the structure, a large air pocket is entrapped, which then undergoes expansion and compression. Meanwhile, a thin horizontal jet creates when the up-rushing water is deflected back by the recurved parapet. These phenomena can well explain the characteristics in the time-histories of pressure, including large-amplitude peaks, negative sub-atmospheric pressure, and oscillations. In the future, we will focus on improving our numerical model with corresponding high-fidelity methods.

## ACKNOWLEDGEMENTS

This work was supported by the National Natural Science Foundation of China (51879159, 52131102), and the National Key Research and Development Program of China (2019YFB1704200), to which the authors are most grateful.

## REFERENCES

Afshar, MA (2010). "Numerical wave generation in OpenFOAM®," Master of Science Thesis, Chalmers University of Technology.

Borsboom, M, and Jacobsen, NG (2021). "A generating-absorbing boundary condition for dispersive waves," *International Journal for Numerical Methods in Fluids*, 93, 2443–2467.

Cao, H, and Wan, D (2017). "Benchmark computations of wave run-up on single cylinder and four cylinders by naoe-FOAM-SJTU solver," *Applied Ocean Research*, 65, 327-337.

Castellino, M, Sammarco, P, Romano, A, Martinelli, L, Ruol, P, Franco, L, and De Girolamo, P (2018a). "Large impulsive forces on recurved parapets under non-breaking waves. A numerical study," *Coastal Engineering*, 136, 1-15.

Castellino, M, Lara, JL, Romano, A, Losada, IJ, and De Girolamo, P (2018b). "Wave loading for recurved parapet walls in non-breaking wave conditions: analysis of the induced impulsive forces," *Coastal Engineering Proceedings*, 1(36), 34-42.

Chen, S, Zhao, W, and Wan, D (2022). "Turbulent structures and characteristics of flows past a vertical surface-piercing finite circular cylinder," *Physics of Fluids*, 34, 015115.

Jacobsen, NG, Fuhrman, DR, and Fredsøe, J (2012). "A wave generation toolbox for the open-source CFD library: OpenFoam®," *International Journal for numerical methods in fluids*, 70(9), 1073-1088.

Kortenhaus, A, Haupt, R, and Oumeraci, H (2002). "Design aspects of vertical walls with steep foreland slopes." *In Breakwaters, Coastal Structures and Coastlines: Proceedings of the International Conference Organized by the Institution of Civil Engineers and Held in London, UK on 26-28 September 2001*, 221-231.

Kortenhaus, A, Pearson, J, Bruce, T, Allsop, NWH, and Van der Meer, JW (2003). "Influence of parapets and recurves on wave overtopping and wave loading of complex vertical walls," *In Proceedings of Coastal Structures*, 369-381.

Liu, S, Gatin, I, Obhrai, C, Ong, MC, and Jasak, H (2019). "CFD simulations of violent breaking wave impacts on a vertical wall using a two-phase compressible solver," *Coastal Engineering*, 154, 103564.

Molines, J, Bayón, A, Gómez-Martín, ME, and Medina, JR (2020). "Numerical study of wave forces on crown walls of mound breakwaters with parapets," *Journal of Marine Science and Engineering*, 8(4), 276.

Ravindar, R, and Sriram, V (2021). "Impact Pressure and Forces on a Vertical Wall with Different Types of Parapet," Journal of Waterway, Port, Coastal, and Ocean Engineering, 147(3), 04021007.

Ravindar, R, Sriram, V, Schimmels, S, and Stagonas, D (2019). "Characterization of breaking wave impact on vertical wall with recurve," *ISH Journal of Hydraulic Engineering*, 25(2), 153-161.

Ravindar, R, Sriram, V, Schimmels, S, and Stagonas, D (2021). "Approaches in Scaling Small-Scale Experiments on the Breaking Wave Interactions with a Vertical Wall Attached with Recurved Parapets," *Journal of Waterway, Port, Coastal, and Ocean Engineering*, 147(6), 04021034.

Rusche, H (2003). "Computational fluid dynamics of dispersed two-phase flows at high phase fractions," PhD Thesis, Imperial College London (University of London).

Shen, Z, Wan, D, and Carrica, PM (2015). "Dynamic overset grids in OpenFOAM with application to KCS self-propulsion and maneuvering," *Ocean Engineering*, 108, 287-306.

Wang, J, and Wan, D (2018). "CFD investigations of ship maneuvering in waves using naoe-FOAM-SJTU Solver," Journal of Marine Science and Application, 17(3), 443-458.

Wang, J, Zhao, W, and Wan, D (2019). "Development of naoe-FOAM-SJTU solver based on OpenFOAM for marine hydrodynamics," Journal of Hydrodynamics, 31(1), 1-20.

Wellens, P, and Borsboom, M (2020). "A generating and absorbing boundary condition for dispersive waves in detailed simulations of free-surface flow interaction with marine structures," Computers and Fluids, 200, 104387.

Weller, HG (2008). "A new approach to VOF-based interface capturing methods for incompressible and compressible flow," OpenCFD Ltd., Report TR/HGW, 4, 35.

Zhao, W, Zou, L, Wan, D, and Hu, Z (2018). "Numerical investigation of vortex-induced motions of a paired-column semi-submersible in currents," *Ocean Engineering*, 164, 272-283.

Zhuang, Y, and Wan, D (2021). "Parametric study of a new HOS-CFD coupling method," *Journal of Hydrodynamics*, 33(1), 43-54.